

Sulfate reducing bacterium *Desulfovibrio vulgaris* caused severe microbiologically influenced corrosion of zinc and galvanized steel

Di Wang^a, Tuba Unsal^{a,b}, Sith Kumseranee^c, Suchada Punpruk^c, Magdy E. Mohamed^d,
Mazen A. Saleh^d, Tingyue Gu^{a,*}

^a Department of Chemical & Biomolecular Engineering, Institute for Corrosion and Multiphase Technology, Ohio University, Athens, 45701, USA

^b Institute of Marine Sciences and Management, Istanbul University, Istanbul, 34134, Turkey

^c PTT Exploration and Production, Bangkok, 10900, Thailand

^d Research and Development Center, Saudi Arabian Oil Company, Dhahran, 31311, Saudi Arabia

ARTICLE INFO

Keywords:

Galvanized steel
Zinc
Corrosion
Sulfate reducing bacteria (SRB)
Biofilm

ABSTRACT

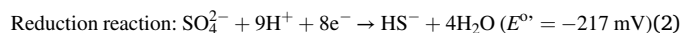
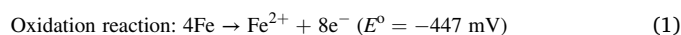
The microbiologically influenced corrosion (MIC) of zinc and galvanized steel caused by a sulfate reducing bacterium (SRB) was investigated. After 7 days of incubation of *Desulfovibrio vulgaris* in 125 mL anaerobic vials (100 mL culture medium) at 37 °C, the sessile cell coverage on the galvanized steel was slightly higher than that on pure zinc: $(1.9 \pm 0.2) \times 10^9$ cells/cm² vs. $(9.0 \pm 1.8) \times 10^8$ cells/cm². The weight losses for galvanized steel and pure zinc were 31.5 ± 2.5 mg/cm² and 35.4 ± 4.5 mg/cm², respectively, which were 10¹ higher than that for carbon steel. The corrosion current densities of galvanized and pure zinc were 25.5 μA/cm² and 100 μA/cm², respectively after the 7-day incubation, confirming that galvanized steel was less prone to SRB MIC despite having a slightly higher sessile cell count. In both cases, the corrosion product was mainly ZnS. Three MIC mechanisms were possible for the severe corrosion against the two metals. Extracellular electron transfer MIC (EET-MIC) was thermodynamically favorable for zinc. Furthermore, in the presence of Zn coupons, H₂ evolution in the headspace was 5.5 times higher than without Zn coupons, which suggested that proton attack and/or H₂S attack also occurred in the corrosion process.

1. Introduction

Zinc and its alloys are often used as sacrificial anodes to protect iron because Zn is more active than Fe (Liu et al., 2017). Galvanized steel is zinc-coated carbon steel used to protect against corrosion (Marder, 2000). Both zinc and galvanized steel are extensively used in automobile, construction and shipbuilding industries (Huda, 2020). When zinc is exposed to the atmosphere, ZnO, Zn(OH)₂ and various basic salts form a passive layer on the zinc surface to give a high resistance to corrosion. Therefore, iron or carbon steel can be protected by coating with a zinc layer against corrosion (Thomas et al., 2012).

Even though zinc and galvanized steel have good anticorrosion properties, microbiologically influenced corrosion (MIC) of zinc can happen because of the metabolic activities of microorganisms like heterotrophic bacteria in aerobic water system and sulfate reducing bacteria (SRB) in anaerobic condition (Bolton et al., 2010; Ilhan-Sungur and Cotuk, 2005; Ilhan-Sungur et al., 2007). SRB are often found in anaerobic environments where sulfate is available. SRB can take sulfate as the

terminal electron acceptor for anaerobic respiration (Jia et al., 2018). Reactions 1 and 2 show the SRB bioenergetics using Fe as electron donor with sulfate acting as electron acceptor when there is a local shortage of other regular electron donors such as organic carbon (Jia et al., 2018; Dou et al., 2019; Unsal et al., 2019).



When Reactions 1 and 2 are coupled together, the redox reaction has a reaction cell potential of +230 mV (at pH 7 as denoted by the apostrophe in E). This positive potential points out that the corrosion reaction is favorable thermodynamically (Xu et al., 2016). SRB biofilms transport extracellular electrons that iron loses across the cell wall to reach the SRB cytoplasm for sulfate reduction (Reguera et al., 2005; Marsili et al., 2008). This cross-cell wall electron transfer process is known as extracellular electron transfer (EET) (Jia et al., 2018). Thus, this kind of MIC is labelled as EET-MIC in MIC science.

* Corresponding author.

E-mail address: gu@ohio.edu (T. Gu).

<https://doi.org/10.1016/j.ibiod.2020.105160>

Received 5 September 2020; Received in revised form 22 November 2020; Accepted 7 December 2020

Available online 13 December 2020

0964-8305/© 2020 Elsevier Ltd. All rights reserved.

Zn^{2+}/Zn has a more negative reduction potential than Fe^{2+}/Fe (Stansbury and Buchanan, 2000). It means that Zn is a more active or energetic metal than Fe, because Zn has a stronger tendency to lose electrons in the oxidation reaction below.



Thus, the direct coupling of zinc oxidation reaction with sulfate reduction is favorable thermodynamically, which leads to EET-MIC in theory. In EET-MIC by SRB, SRB sessile cells harvest energy by utilizing extracellular electrons from an energetic metal such as Fe and Zn for sulfate reduction (Jia et al., 2018).

Zinc can also be corroded by proton when the zinc's passive film is damaged by SRB. At pH 7, $2\text{H}^+/\text{H}_2$ potential ($E^{\circ} = -414 \text{ mV}$) is not much higher than that for Fe^{2+}/Fe ($E^{\circ} = -447 \text{ mV}$), making proton attack of carbon steel insignificant. However, the $2\text{H}^+/\text{H}_2$ potential is much higher than that for Zn^{2+}/Zn ($E^{\circ} = -763 \text{ mV}$) because Zn is much more active than Fe. This means Zn oxidation (Reaction 3) coupled with proton reduction (Reaction 4) has a large thermodynamic driving force at pH 7.



Zinc can also be corroded by H_2S which is a metabolite produced by SRB. This kind of corrosion belongs to metabolite MIC (M-MIC) (Wang et al., 2020a). In Reaction 5, proton is reduced to produce H_2 gas, just like in zinc hydrolysis corrosion above (Svensson and Johansson, 1996). This means in both H^+ and H_2S corrosion mechanisms, H^+ serves as the electron acceptor.



In the past, many studies reported that zinc is toxic to bacteria (Utigkar et al., 2003; Poulson et al., 1997). On the other hand, some studies also reported that bacterial biofilms formed on zinc surfaces which led to MIC of zinc (Ilhan-Sungur et al., 2007, 2015). Zinc toxicity can be detoxified by SRB through ZnS precipitation, which removes the microbiocidal Zn ions from the SRB broth. This is similar to SRB detoxification of microbiocidal Cu ions (Dou et al., 2018). Copper MIC by SRB follows the M-MIC mechanism with hydrogen evolution and Cu_2S precipitation (Dou et al., 2018; Li et al., 2018).

Galvanized steel is produced by dipping carbon steel in a molten zinc liquid to form a thin layer of zinc that offers protection against corrosion. Despite the protection of the passive film which is usually effective against abiotic corrosion, microbial biofilms can damage the film, leading to MIC. Because the dipping solution often contains small amounts of other elements in addition to Zn, it is worthwhile to compare pure zinc and galvanized steel in SRB MIC.

In this work, under strictly anaerobic condition, the MIC of zinc and galvanized steel caused by SRB was investigated and compared. Sessile cell count, corrosion weight loss, pit depth, LPR (linear polarization resistance) and potentiodynamic polarization data were used to investigate their MIC behaviors.

2. Materials and methods

2.1. Metals, culture medium and bacterium

Pure zinc and galvanized steel coupons (1.0 cm × 1.0 cm exposed surface) were used. The metals were donated by Taiyuan Iron & Steel Group. (Taiyuan, Shanxi Province, China). EDS (energy-dispersive X-ray spectroscopy) results suggested no detectable impurities in the pure zinc, and the zinc coating in the galvanized steel contained 0.5% (w/w) Si in addition to Zn. Only the top coupon surfaces were in contact with the culture medium. All other surfaces were coated with a protective Teflon paint. The coupon surface was dried for 1 h and then baked in an oven at 90 °C for 2 h for good bonding. Before testing, pure zinc coupons were polished to 600 grit. Galvanized steel coupons were not polished to

avoid damaging the thin zinc layer (45 μm thickness). Afterwards, all the coupons were sanitized with absolute isopropanol and air dried with UV lighting on for at least 20 min.

Desulfovibrio vulgaris (ATCC 7757) was cultured in standard ATCC 1249 medium with 200 ppm Fe^{2+} by mass. In it, sodium lactate was used as organic carbon for the growth of SRB. Sodium citrate was used as a chelator to increase Fe^{2+} bioavailability for better SRB growth (Jia et al., 2019). One or two drops of 5% (w/w) NaOH solution or 5% HCl solution was used to adjust the pH of ATCC 1249 medium to 7.0 before autoclaving. In a N_2 -filled glovebox, 1 mL L-cysteine stock solution (10,000 ppm), which was filter-sterilized, was pipetted to each 125 mL anaerobic vial with 1 mL *D. vulgaris* seed culture, 98 mL ATCC 1249 culture medium, and 3 replicate coupons.

2.2. Sessile cell counting and biofilm visualization

Coupons were retrieved for sessile cell count analysis after incubation lasting for 7 days. The liquid modified Postgate's B culture medium was used for enumerating sessile SRB cell count with most probable number (MPN) method. A total of three coupons from 3 replicate 125 mL anaerobic vials were employed to obtain a sessile cell count data point for improved MPN accuracy (Sutton, 2010). Information on how to collect SRB sessile cell count data can be found in a previous report (Jia et al., 2017a; Wang et al., 2020b). The live and dead sessile SRB cells on zinc and galvanized steel were visualized under confocal laser scanning microscopy (CLSM) (Model LSM 510, Carl Zeiss, Jena, Germany). The experimental procedure for the sample preparation can be found elsewhere (Jia et al., 2017b).

2.3. H_2 concentration

The H_2 concentration in the 24 mL headspace of each 125 mL vial containing 3 zinc coupons was measured every day during the incubation period using a H_2 gas detector (Model FD-90A, Forensics Detectors, Palos Verdes Peninsula, CA, USA). Ten mL headspace gas was extracted from each 125 mL anaerobic vial by a syringe and injected into a sealed 250 mL vial filled with 1 atm air for diluting the H_2 concentration. Then, 40 mL gas from the 250 mL dilution vial was withdrawn and directly injected into the H_2 detector's sampling port without a tubing extension. H_2S was not scrubbed because it did not interfere with the electrochemical H_2 sensor's readings in this work.

2.4. Corrosion analysis

The zinc and galvanized steel coupons were analyzed using a scanning electron microscope (SEM, Model JSM-6390, JEOL, Tokyo, Japan). The protocol used by Jia et al. (2017b) to prepare coupon surfaces for biofilm imaging under SEM was adopted. The corrosion products and biofilms were removed according to ASTM G1-03 (2003) before corrosion analysis. The pit depth profile was scanned under a profilometer (Model ALC 13, Alicona Imaging GmbH, Austria.). The corrosion product films were analyzed using a powder X-ray diffraction (XRD) (Model MiniFlex, Rigaku, Tokyo, Japan).

2.5. Electrochemical measurements

Several electrochemical tests were carried out with a potentiostat (PCI4/750, Gamry, Warminster, PA, USA) for open circuit potential (OCP), linear polarization resistance (LPR) and potentiodynamic polarization (PDP). These tests were performed in 450 mL glass cells filled with 300 mL ATCC 1249 medium and 145 mL headspace with and without SRB inoculation. For the counter electrode, a thin 1 cm² platinum plate (was employed, and for the reference, a saturated calomel electrode (SCE) was adopted. Pure zinc and galvanized steel coupons (1 cm² surface) were used as working electrodes separately. The scan rate for the daily LPR scans was 0.167 mV/s from -10 mV to +10 mV vs.

(OCP). After the 7-day anaerobic incubation, PDP scans were conducted at 0.167 mV/s from -250 mV to $+250$ mV (vs. OCP).

3. Results

3.1. Sessile cell counts and biofilm visualization

The SRB sessile cell counts on the surfaces of galvanized steel and zinc were found to be $(1.9 \pm 0.2) \times 10^9$ cells/cm² and $(9.0 \pm 1.8) \times 10^8$ cells/cm², respectively. The high sessile cell counts mean that dense SRB biofilms were formed on both metals, which could be visualized under CLSM (Fig. S1).

3.2. Corrosion analysis

Fig. 1 displays SEM images of corroded pure zinc and galvanized steel coupon surfaces. Pure zinc is usually corroded uniformly instead of severe pitting corrosion (Juzeliūnas et al., 2007), but pits and cracks are clearly observed on the zinc surface in Fig. 1A. In comparison, the corroded galvanized steel surface appears far more uniform in Fig. 1B.

The abiotic weight losses were (1.4 ± 0.2) mg/cm² for zinc and (4.6 ± 0.3) mg/cm² for galvanized steel. In the *D. vulgaris* broth, the weight loss for galvanized steel was slightly lower than that for pure zinc (31.5 ± 4.5 mg/cm² vs. 35.4 ± 2.5 mg/cm²). The pH values of SRB broths for all conditions were slightly above 7 (Fig. 2). XRD data indicated that the main corrosion product for Zn MIC by SRB in this work was ZnS (Fig. S2), consistent with all the three aforementioned MIC mechanisms.

Fig. 3 shows the pitting profiles on the coupons after surface cleaning. The abiotic coupons of the two metals show a wavy surface attributed to surface roughness without deep pits in Fig. 3(A, B). The biotic maximum pit depths were 29.2 μm and 63.0 μm for galvanized steel and pure zinc after the 7-day incubation, respectively.

3.3. Electrochemical results

Fig. 4 provides transient OCP behavior. The OCP values of the pure zinc and galvanized steel coupons were both around -1050 mV in the bacterium-free medium and kept steady. After 2 days, the OCP became more positive in the SRB broth for both metals. After 2.5 days, the biotic galvanized steel coupon OCP was more positive than the biotic pure zinc OCP until the end of the incubation.

During the 7-day incubation, the abiotic polarization resistance (R_p) curve (Fig. 5) was steady at 3.2 kΩ cm² and 2.9 kΩ cm² for pure zinc and galvanized steel, respectively. A lower R_p means a higher corrosion rate. The R_p values of zinc and galvanized steel were lower than that (18 kΩ cm²) for carbon steel (Jia et al., 2018) and this comparison can explain the high weight losses in the abiotic conditions. The biotic pure zinc's R_p

was slightly lower than that of biotic galvanized steel, indicating a higher corrosion rate for pure zinc.

Fig. 6 shows the potentiodynamic polarization curves. The anodic (β_a) and cathodic (β_c) Tafel slopes, corrosion potential (E_{corr}) and current density (i_{corr}) from potentiodynamic polarization curves are displayed in Table 1. The E_{corr} of the abiotic pure zinc coupon (-884 mV vs. SCE) was less negative than that of biotic zinc (-956 mV vs. SCE). The i_{corr} of abiotic pure zinc coupon was 5.4 μA/cm². The i_{corr} values were found to be 23.5 μA/cm² and 100 μA/cm² for biotic galvanized steel and pure zinc, respectively (Table 1).

4. Discussion

Although the galvanized steel was not polished to avoid damaging its thin Zn coating, its relatively rougher surface had only a marginally higher sessile cell count. Some studies showed that zinc ions at higher concentrations may hamper the metabolic activities of microorganisms including SRB (Utgikar et al., 2003). A high zinc ion concentration inhibits electron transport in microbial respiration. Radhika et al. showed that the concentration of zinc ion lethal to SRB is about 210 ppm (w/w) (Radhika et al., 2006). Also, Azabou et al. reported that a Zn²⁺ concentration of 400 mg/L inhibits the activity of SRB (Azabou et al., 2007). The apparent lack of zinc toxicity in this work was because the zinc ion concentration in the culture medium was not significant initially. During the corrosion process, the released zinc ions were promptly precipitated by sulfide because ZnS solubility product constant is very small ($K_{\text{sp}} = 2 \times 10^{-25}$ at 25 °C) (SenGupta, 2017).

The abiotic weight loss in this study was much higher than the typical abiotic weight loss for carbon steel (0.3 mg/cm²) after 7 days of incubation (Wang et al., 2020a). There was 0.018 mg/cm² weight loss of carbon steel caused by proton reduction calculated from the H₂ concentration (1010 ppm) in the headspace measured in the abiotic control condition (Wang et al., 2020a), so the much larger abiotic weight loss of zinc and galvanized steel compared to Fe could be contributed to proton attack with H₂ evolution because Zn is more active than Fe.

The MIC weight losses of zinc in the *D. vulgaris* broth in Fig. 2 are 10X higher than the typical C1018 carbon steel weight loss in *D. vulgaris* broth reported by Jia et al. (2019). The SRB sessile cell count on the zinc surface is 10¹ higher than the SRB sessile cell counts on the carbon steel in the literature (Jia et al., 2019). This helps explain the 10X higher zinc and galvanized steel weight losses.

At pH slightly above 7, proton reduction or water reduction attack would be insignificant in carbon steel corrosion. However, this attack could be significant against Zn with passive film damage by SRB because Zn is far more active than Fe. It was found that the peak H₂ concentration in the headspace with 3 zinc coupons in the SRB broth was 6900 ppm (v/v), which was 5.5 times higher than that without any coupons.

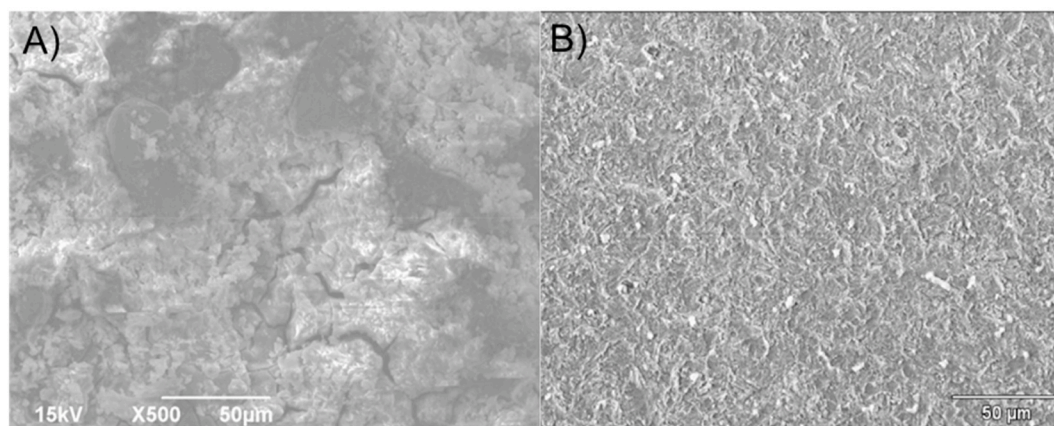


Fig. 1. SEM images of coupon surfaces (after removing biofilm and corrosion products) after 7-day incubation: A) pure zinc, and B) galvanized steel.

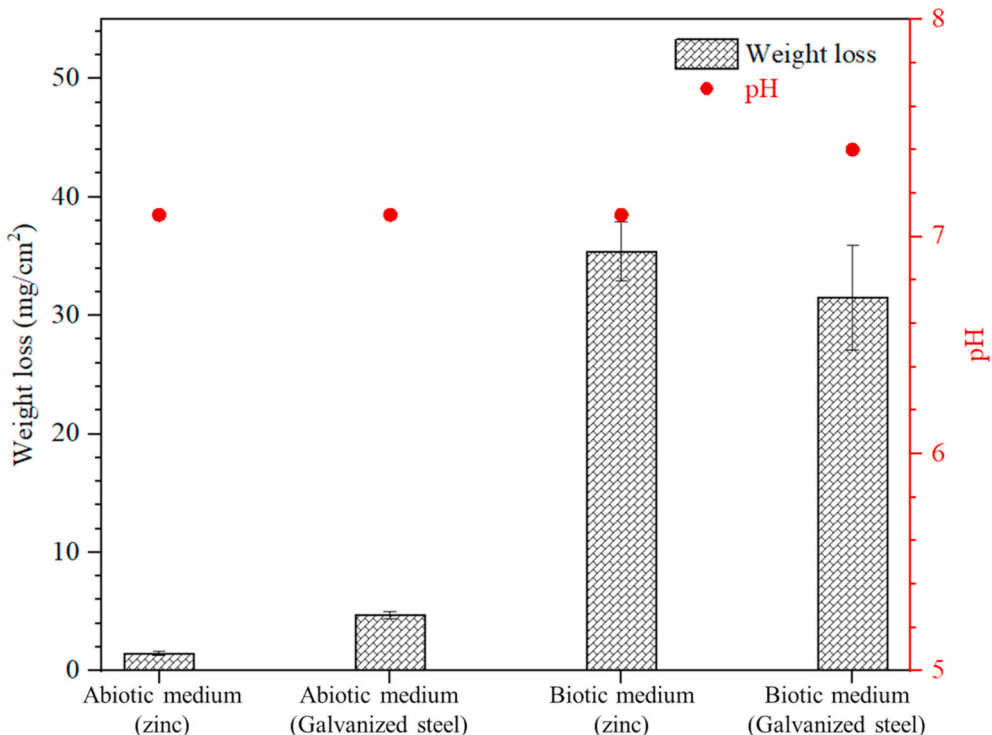


Fig. 2. Weight losses (columns) and broth pH values (circles) after 7-day incubation in anaerobic vials. (Standard deviation was calculated from 4 independent coupons.)

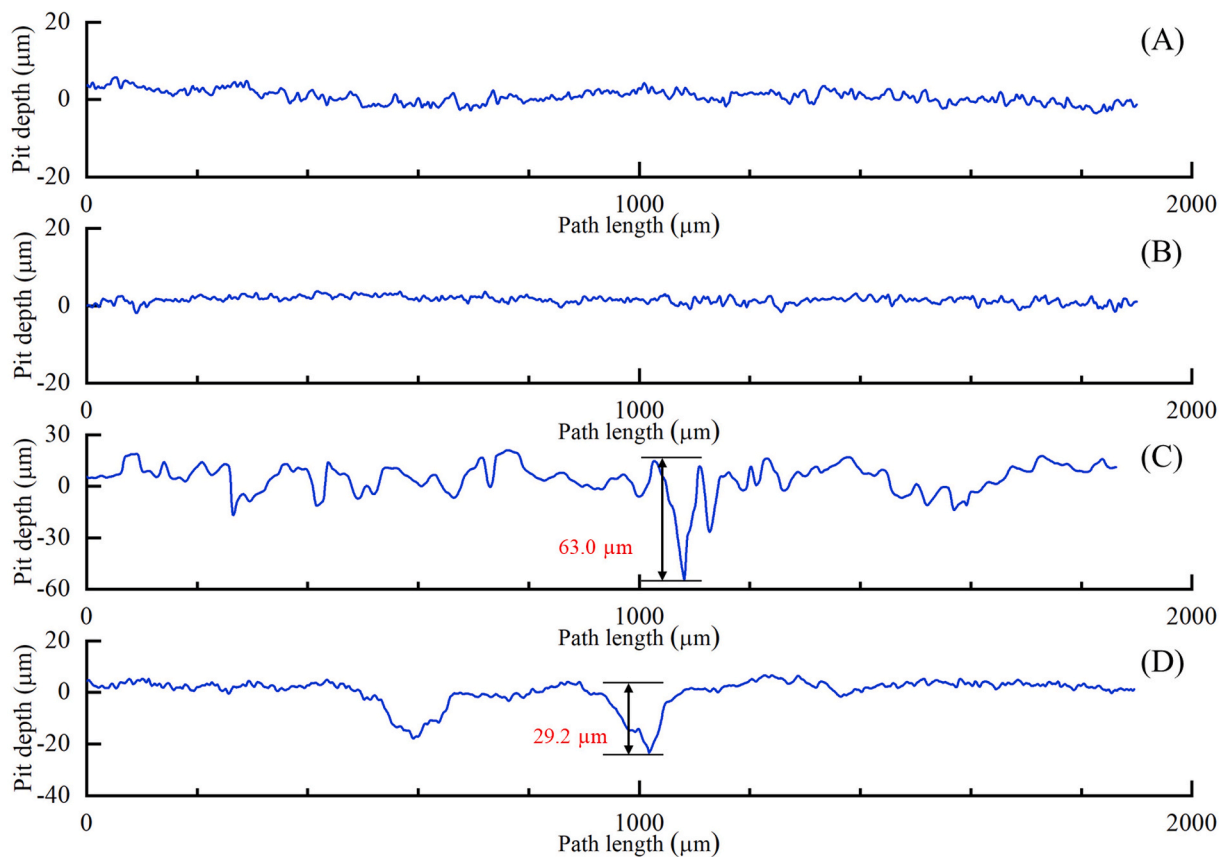


Fig. 3. Pitting profiles after 7-day incubation in anaerobic vials: (A) abiotic pure zinc, (B) abiotic galvanized steel, (C) biotic pure zinc, and (D) biotic galvanized steel.

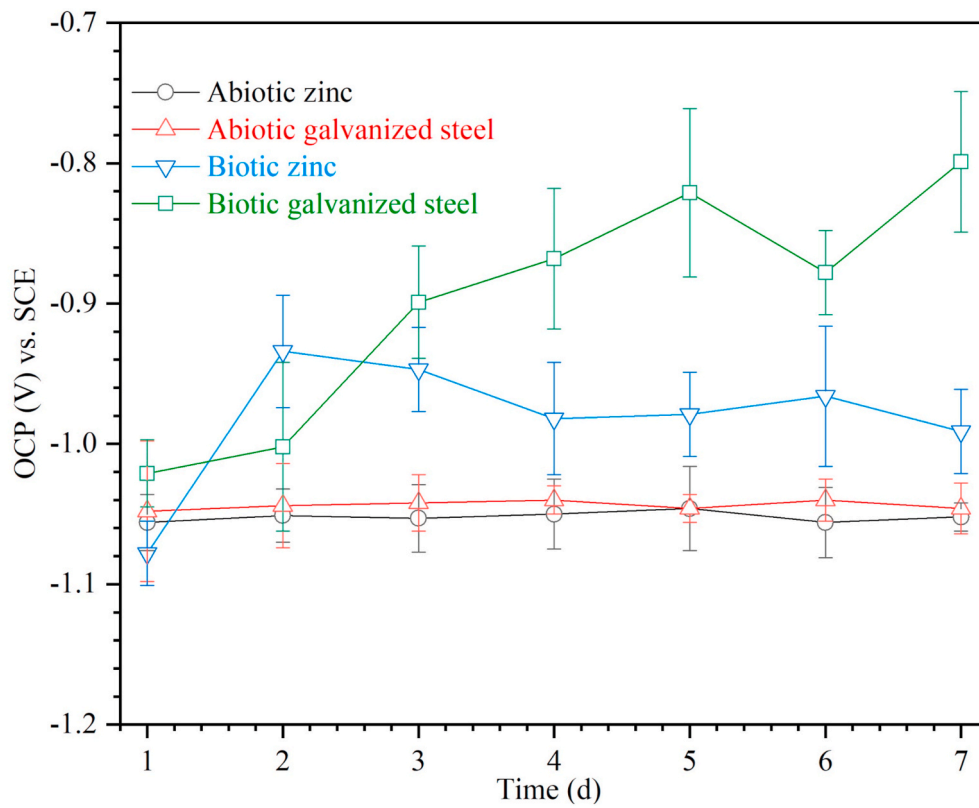


Fig. 4. Variations of OCP vs. time during 7-day incubation in 450 mL anaerobic glass cells.

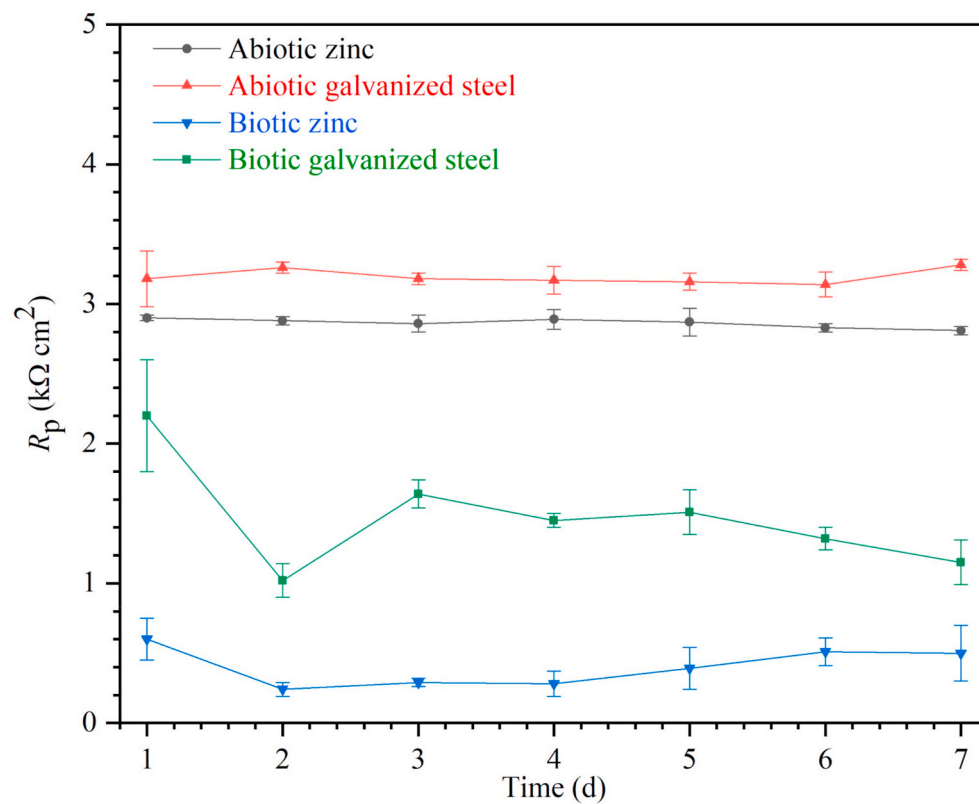


Fig. 5. R_p values from LPR during 7-day incubation.

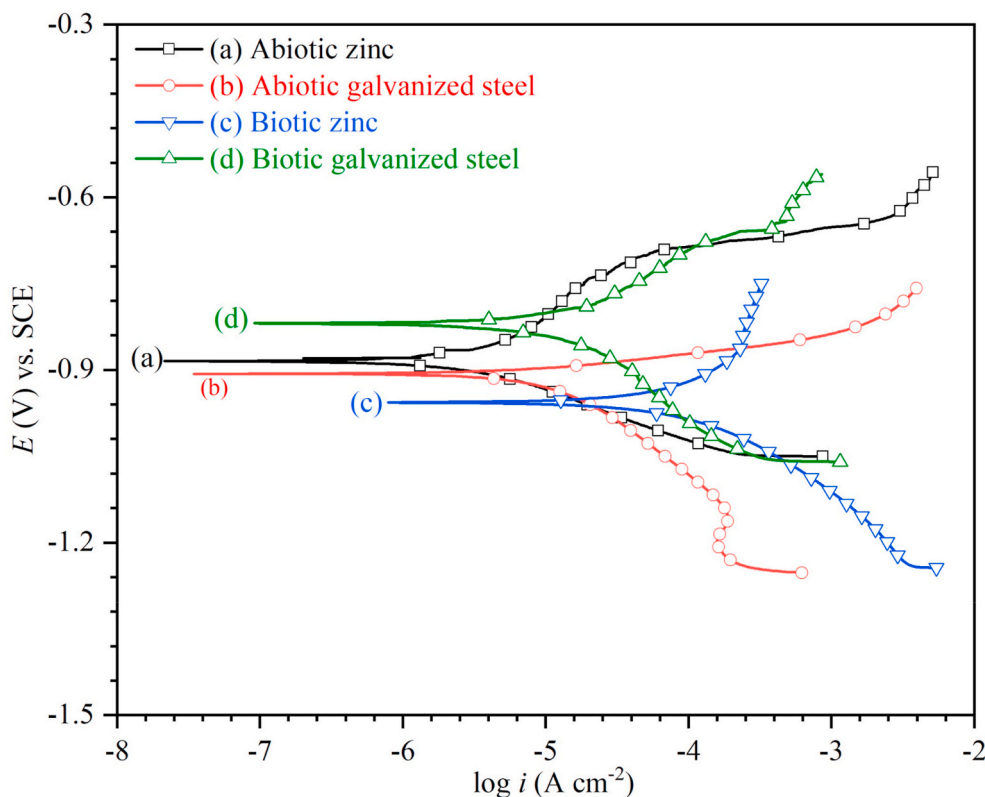


Fig. 6. Potentiodynamic polarization curves at the end of 7-day incubation.

Table 1

Fitted electrochemical parameters from Tafel analysis of potentiodynamic polarization curves obtained at the end of 7-day incubation.

Parameter	Abiotic		Biotic	
	Pure zinc	Galvanized steel	Pure zinc	Galvanized steel
β_a (mV/dec)	125	29	128	184
β_c (mV/dec)	253	119	202	283
i_{corr} ($\mu\text{A}/\text{cm}^2$)	5.4	6.9	100	23.5
E_{corr} (mV) vs. SCE	-884	-906	-956	-818

This suggests that H_2 evolution from proton reduction at pH 7 (Reaction 4 or 5) was very significant. Thus, hydrolysis contributed to zinc corrosion. The 6900 ppm H_2 in the headspace was stoichiometrically equivalent to a very small weight loss of $0.14 \text{ mg}/\text{cm}^2$. However, some H_2 produced by corrosion could be consumed by *D. vulgaris* metabolism (Wang et al., 2020a). Thus a stoichiometric analysis could not be carried out. H_2 evolution could be the result of M-MIC of Zn by H^+ (Reaction 4) and H_2S (Reaction 5). H^+ was the electron acceptor in both cases. In the water hydrolysis of Zn case, the released Zn^{2+} would react with S^{2-} . Thus, the net outcome was the same as when H_2S was present.

In the presence of *D. vulgaris*, pure zinc pitting corrosion (Fig. 3C) increased greatly compared to the abiotic coupon. The SRB pitting corrosion on pure zinc was more severe than on galvanized steel, which is consistent with pit images under SEM (Fig. 1). The maximum pit depth of $29.2 \mu\text{m}$ was smaller than the zinc coating thickness ($45 \mu\text{m}$) on the galvanized steel in SRB MIC, despite the observation that galvanized steel had a slightly higher sessile cell count. Thus, the less severe SRB weight loss and pitting on the galvanized steel compared with pure zinc could be contributed to the alloying elements (most noticeably 0.5% Si) in the dipping solution, which were intended to improve corrosion protection.

A parameter called relative pitting severity (*RPS*) can reflect the importance of pitting corrosion relative to uniform (general) corrosion.

For *D. vulgaris* MIC against carbon steel, *RPS* is significantly larger than 1, which means pitting corrosion is more important than uniform corrosion. The *RPS* values were 1.3 and 0.6 for zinc and galvanized steel, respectively in this work. These values show that uniform corrosion was more severe than pitting corrosion for galvanized steel, but it was the opposite for pure zinc, as evidenced by SEM images (Fig. 1).

OCP is a thermodynamic parameter. A lower OCP corresponds to a higher thermodynamic tendency for the metal (working electrode) to be corroded. The two biotic OCP curves in Fig. 4 exhibit a trend suggesting that zinc was more prone to corrosion. This seems consistent with weight loss and pitting data. However, for each metal, its abiotic OCP curve suggests that the metal was more prone to corrosion abiotically than biotically, which is obviously wrong. This kind of misleading OCP trend is common for complicated SRB corrosion system (Jia et al., 2018; Liu et al., 2018). A thermodynamic advantage can be offset by a slow corrosion kinetic process. Furthermore, a corrosion process with a large thermodynamic tendency but severe kinetic handicap may be replaced by a different process with a small thermodynamic tendency but much faster kinetics. Thus, OCP data should be interpreted with caution when the liquid environment is complicated. In comparison, MIC literature has repeatedly confirmed that kinetic electrochemical measurements such as LPR, potentiodynamic polarization and electrochemical impedance spectrometry (EIS) reliably corroborate coupon weight loss and pitting trends even when OCP shows the wrong trend (Jia et al., 2018; Liu et al., 2018).

The i_{corr} data in Table 1 confirmed that pure zinc was more prone to SRB MIC. Note that the weight loss data indicated cumulative corrosion for the 7-day incubation, but the i_{corr} data were only for the end of the test. It is a common practice because potentiodynamic polarization scans should be done only once at the end owing to the fact that coupon surface properties can be altered by the wide voltage range. It is worthwhile to note that the ranking of E_{corr} values differed considerably from that for OCP in Fig. 4. Although OCP and E_{corr} are both considered thermodynamic data in electrochemical analysis, OCP is measured when

there was no corrosion current, while E_{corr} , often confused with OCP, is measured with corrosion ongoing. Nonetheless, corrosion outcome relies on both thermodynamic driving force and kinetics. The OCP and E_{corr} trends both were inconsistent with weight loss and pit depth trends. This means for a complicated biotic system, their trends may not be reliable in corrosion outcome analysis. Instead, kinetic data such as LPR and Tafel data should be used. In this work, Fig. 4 shows that OCP shifted upward considerably in the presence of SRB. It is known that H_2S can shift OCP up greatly for some metals (Chen et al., 2010; Jia et al., 2018). Despite the impact of H_2S on OCP, the kinetic LPR and Tafel results were proven reliable in this work because they were consistent with weight loss and pit depth data trends. This has been demonstrated in electrochemical testing of MIC against carbon steel, copper and other metals in the literature as well (Jia et al., 2018; Wang et al., 2020a).

5. Conclusion

D. vulgaris formed healthy biofilms on zinc and galvanized steel after the 7-day incubation at 37 °C, causing severe corrosion. The biotic weight losses for zinc coupon and galvanized steel were 35.4 ± 4.3 and $31.5 \pm 2.5 \text{ mg/cm}^2$, respectively, which were 10X larger than typical carbon steel weight loss in SRB MIC. Pit depths of coupons were found to be 63.0 μm and 29.2 μm for pure zinc and galvanized steel, respectively after 7 days of incubation with SRB. The RPS values showed that the pitting corrosion was more severe than uniform corrosion for zinc MIC caused by SRB, while the opposite was true for galvanized steel. The electrochemical results, namely R_p and i_{corr} , confirmed the weight loss trend. H_2 evolution data supported Zn hydrolysis corrosion and Zn corrosion by H_2S . Despite having a slightly higher sessile cell count, corrosion data suggested that galvanized steel was less prone to SRB MIC.

Declaration of competing interest

The authors declare that they have no known competing financial interests or personal relationships that could have appeared to influence the work reported in this paper.

Acknowledgements

We appreciate the help from Prof. Martin Kordesch for the use of SEM and XRD in his lab. This work was supported by PTT Exploration and Production of Thailand, Saudi Aramco, and Chinese Society for Corrosion and Protection. Parts of this work were taken with permission from Corrosion/2020 Conference Paper 2020–14537.

Appendix A. Supplementary data

Supplementary data to this article can be found online at <https://doi.org/10.1016/j.ibiod.2020.105160>.

References

- ASTM G1-03, 2003. Standard Practice for Preparing, Cleaning and Evaluating Corrosion Test Specimens.
- Azabou, S., Mechichi, T., Sayadi, S., 2007. Zinc precipitation by heavy-metal tolerant sulfate-reducing bacteria enriched on phosphogypsum as a sulfate source. *Miner. Eng.* 20, 173–178.
- Bolton, N., Critchley, M., Fabien, R., Cromar, N., Fallowfield, H., 2010. Microbially influenced corrosion of galvanized steel pipes in aerobic water systems. *J. Appl. Microbiol.* 109, 239–247.
- Chen, J., Qin, Z., Shoosmith, D.W., 2010. Kinetics of corrosion film growth on copper in neutral chloride solutions containing small concentrations of sulfide. *J. Electrochem. Soc.* 157, C338–C345.
- Dou, W., Jia, R., Jin, P., Liu, J., Chen, S., Gu, T., 2018. Investigation of the mechanism and characteristics of copper corrosion by sulfate reducing bacteria. *Corros. Sci.* 144, 237–248.
- Dou, W., Liu, J., Cai, W., Wang, D., Jia, R., Chen, S., Gu, T., 2019. Electrochemical investigation of increased carbon steel corrosion via extracellular electron transfer by a sulfate reducing bacterium under carbon source starvation. *Corros. Sci.* 150, 258–267.
- Huda, Z., 2020. *Metallurgy for Physicists and Engineers: Fundamentals, Applications, and Calculations*. CRC Press.
- Ilhan-Sungur, E., Cansever, N., Cotuk, A., 2007. Microbial corrosion of galvanized steel by a freshwater strain of sulphate reducing bacteria (*Desulfovibrio* sp.). *Corros. Sci.* 49, 1097–1109.
- Ilhan-Sungur, E., Cotuk, A., 2005. Characterization of sulfate reducing bacteria isolated from cooling towers. *Environ. Monit. Assess.* 104, 211–219.
- Ilhan-Sungur, E., Unsal, T., Cansever, N., 2015. Microbiologically influenced corrosion of galvanized steel by *Desulfovibrio* sp. and *Desulfosporosinus* sp. in the presence of Ag–Cu ions. *Mater. Chem. Phys.* 162, 839–851.
- Jia, R., Tan, J.L., Jin, P., Blackwood, D.J., Xu, D., Gu, T., 2018. Effects of biogenic H_2S on the microbiologically influenced corrosion of C1018 carbon steel by sulfate reducing *Desulfovibrio vulgaris* biofilm. *Corros. Sci.* 130, 1–11.
- Jia, R., Wang, D., Jin, P., Unsal, T., Yang, D., Yang, J., Xu, D., Gu, T., 2019. Effects of ferrous ion concentration on microbiologically influenced corrosion of carbon steel by sulfate reducing bacterium *Desulfovibrio vulgaris*. *Corros. Sci.* 153, 127–137.
- Jia, R., Yang, D., Al-Mahamedh, H.H., Gu, T., 2017a. Electrochemical testing of biocide enhancement by a mixture of D-amino acids for the prevention of a corrosive biofilm consortium on carbon steel. *Ind. Eng. Chem. Res.* 56, 7640–7649.
- Jia, R., Yang, D., Li, Y., Xu, D., Gu, T., 2017b. Mitigation of the *Desulfovibrio vulgaris* biofilm using alkylidimethylbenzylammonium chloride enhanced by d-amino acids. *Int. Biodeterior. Biodegrad.* 117, 97–104.
- Juzeliūnas, E., Ramanauskas, R., Lugauskas, A., Leinartas, K., Samulevičienė, M., Sudavičius, A., Juskešas, R., 2007. Microbially influenced corrosion of zinc and aluminium—two-year subjection to influence of *Aspergillus niger*. *Corros. Sci.* 49, 4098–4112.
- Li, Y., Xu, D., Chen, C., Li, X., Jia, R., Zhang, D., Sand, W., Wang, F., Gu, T., 2018. Anaerobic microbiologically influenced corrosion mechanisms interpreted using bioenergetics and bioelectrochemistry: a review. *J. Mater. Sci. Technol.* 34, 1713–1718.
- Liu, H., Gu, T., Zhang, G., Liu, H., Cheng, Y.F., 2018. Corrosion of X80 pipeline steel under sulfate-reducing bacterium biofilms in simulated CO_2 -saturated oilfield produced water with carbon source starvation. *Corros. Sci.* 136, 47–59.
- Liu, S., Zhao, X., Zhao, H., Sun, H., Chen, J., 2017. Corrosion performance of zinc coated steel in seawater environment. *Chin. J. Oceanol. Limnol.* 35, 423–430.
- Marder, A.R., 2000. The metallurgy of zinc-coated steel. *Prog. Mater. Sci.* 45, 191–271.
- Marsili, E., Baron, D.B., Shikhare, I.D., Coursolle, D., Gralnick, J.A., Bond, D.R., 2008. *Shewanella* secretes flavins that mediate extracellular electron transfer. *Proc. Natl. Acad. Sci.* 105, 3968–3973.
- Poulsen, S.R., Colberg, P.J., Drever, J.I., 1997. Toxicity of heavy metals (Ni, Zn) to *Desulfovibrio desulfuricans*. *Geomicrobiol. J.* 14, 41–49.
- Radhika, V., Subramanian, S., Natarajan, K.A., 2006. Bioremediation of zinc using *Desulfotomaculum nigrificans*: bioprecipitation and characterization studies. *Water Res.* 40, 3628–3636.
- Reguera, G., McCarthy, K.D., Mehta, T., Nicoll, J.S., Tuominen, M.T., Lovley, D.R., 2005. Extracellular electron transfer via microbial nanowires. *Nature* 435, 1098–1101.
- SenGupta, A.K., 2017. *Ion Exchange in Environmental Processes: Fundamentals, Applications and Sustainable Technology*. John Wiley & Sons.
- Stansbury, E.E., Buchanan, R.A., 2000. *Fundamentals of Electrochemical Corrosion*. ASM international.
- Sutton, S., 2010. The most probable number method and its uses in enumeration, qualification, and validation. *J. Valid. Technol.* 16, 35–38.
- Svensson, J.-E., Johansson, L.-G., 1996. The synergistic effect of hydrogen sulfide and nitrogen dioxide on the atmospheric corrosion of zinc. *J. Electrochem. Soc.* 143, 51.
- Thomas, S., Birbilis, N., Venkatraman, M.S., Cole, I.S., 2012. Corrosion of zinc as a function of pH. *Corrosion* 68, 015009–1.
- Unsal, T., Jia, R., Kumseranee, S., Punpruk, S., Gu, T., 2019. Laboratory investigation of microbiologically influenced corrosion of carbon steel in hydrotest using enriched artificial seawater inoculated with an oilfield biofilm consortium. *Eng. Fail. Anal.* 100, 544–555.
- Utgikar, V.P., Tabak, H.H., Haines, J.R., Govind, R., 2003. Quantification of toxic and inhibitory impact of copper and zinc on mixed cultures of sulfate-reducing bacteria. *Biotechnol. Bioeng.* 82, 306–312.
- Wang, D., Liu, J., Jia, R., Dou, W., Kumseranee, S., Punpruk, S., Li, X., Gu, T., 2020a. Distinguishing two different microbiologically influenced corrosion (MIC) mechanisms using an electron mediator and hydrogen evolution detection. *Corros. Sci.* 177, 108993.
- Wang, D., Ramadan, M., Kumseranee, S., Punpruk, S., Gu, T., 2020b. Mitigating microbiologically influenced corrosion of an oilfield biofilm consortium on carbon steel in enriched hydrotest fluid using 2,2-dibromo-3-nitropropionamide (DBNPA) enhanced by a 14-mer peptide. *J. Mater. Sci. Technol.* 57, 146–152.
- Xu, D., Li, Y., Gu, T., 2016. Mechanistic modeling of biocorrosion caused by biofilms of sulfate reducing bacteria and acid producing bacteria. *Bioelectrochemistry* 110, 52–58.